

Final Draft
of the original manuscript:

Smazna, D.; Shree, S.; Polonskyi, O.; Lamaka, S.; Baum, M.; Zheludkevich, M.;
Faupel, F.; Adelung, R.; Kumar Mishra, Y.:

**Mutual interplay of ZnO micro- and nanowires and methylene blue during
cyclic photocatalysis process.**

In: Journal of Environmental Chemical Engineering. Vol. 7 (2019) 2, 103016.

First published online by Elsevier: 14.03.2019

<https://dx.doi.org/10.1016/j.jece.2019.103016>

Mutual Interplay of ZnO Micro- and Nanowires and Methylene Blue during Cyclic Photocatalysis Process

Daria Smazna^a, Sindu Shree^a, Oleksandr Polonskyi^b, Sviatlana Lamaka^c, Martina Baum^a, Mikhail Zheludkevich^c, Franz Faupel^b, Rainer Adelung^a, Yogendra Kumar Mishra^{a*}

^aFunctional Nanomaterials, Institute for Materials Science, Kiel University, Kaiserstr. 2, D-24143, Kiel, Germany

^bChair for Multicomponent Materials, Institute for Materials Science, Kiel University, Kaiserstr. 2, D-24143, Kiel, Germany

^cMagIC - Magnesium Innovation Center, Department of Corrosion and Surface Technology

Helmholtz-Zentrum Geesthacht, Max-Planck-Str. 1, D – 21502, Geesthacht, Germany

Corresponding Author:

PD Dr. habil. Yogendra Kumar Mishra

Email: ykm@tf.uni-kiel.de

Abstract

Water purification through photocatalysis is the most important requirements due to the increased health, environmental and energy conservation concerns. Metal oxides nanostructures have played a very prominent role in this direction. ZnO is a promising material in terms of nanostructuring and photocatalysis. This study presents a unique easy-to-follow synthesis method for ZnO micro- and nanowires by a flame- based approach. The photocatalytic activity of these grown ZnO nano- and microwires against methylene blue (MB) has been investigated in detail and a possible decomposition pathway is proposed. During repeated photocatalysis, a significant improvement in the decomposition rate was achieved which is mainly attributed to surface modifications of the ZnO wires due to the reaction with MB as confirmed by Raman-spectroscopic and X-ray photoelectron spectroscopy (XPS) investigations. The impact of the MB over involved nanostructures is thus an important aspect for the efficiency of the photocatalysis which is briefly presented here.

Keywords

Photocatalysis; ZnO micro- and nanowires; flame growth; surface nanostructuring; photo-corrosion

1. Introduction

Industrial progress has provided several human friendly utilities in every field however, simultaneously it has created an enormous amount of chemical waste which is polluting the natural water and the surrounding environment.[1–5] Specially in the last two decades, the amount of dye pollutant remaining into the natural occurring water bodies has tremendously increased because of an abrupt expansion of mass production.[6,7] This points out the absolute necessity for developing efficient water purification methods with high efficiency. Photocatalytic degradation of the dye[1] and adsorptions of contaminants[8–10] are the two most versatile strategies for water purification technologies. Both of these methods involve different material forms such as porous nanomembranes and nanoparticle.[4,5]. However, only adequate nanomaterials with well-defined shapes are mainly relevant for photocatalysis.[11–13] Therefore, a non-toxic nanomaterial based photocatalytic approach for water purification is a key requirement along with being user friendly, cost-effectiveness, rapid system and scalability, etc. Scientific community has been focused in the direction of nanomaterial-based photocatalysis for decomposing organic dyes.[14] The retractability of such nanoparticles is another challenge as it is complicated and requires either advanced filtering techniques or centrifugation process (which does not guarantee their complete removal). For purification of large water volumes, the water has to pass through the decomposition cells and those cells have to be used multiple times. Therefore, in the nanopowder based photocatalysis systems, the retractability, reusability, large scale production (nanomaterials are often expensive), etc. are still very important open challenges.

Material choice becomes rather very important when it comes to nanomaterials based photocatalysis. Metal oxide semiconductors [14–16] are probably the most relevant candidates. Among all, the TiO_2 is particularly well known for its use in photocatalytic water purification[17,18] however its long recovery time between photocatalytic cycles has been a major drawback.[19] Therefore, zinc oxide (ZnO) due to its unique physical, chemical, and biocompatibility features has been widely utilized for photocatalytic degradation of dyes.[11] ZnO is a direct bandgap semiconductor (~ 3.37 eV), it exhibits very unique defect chemistry.[11] These defects interestingly introduce states within the ZnO bandgap opening the possibility of visible light absorption and corresponding photocatalysis.[11,20,21] Because of its hexagonal-wurtzite crystal structure, nanostructures of almost any desired complex shape can be grown by wet chemistry and many other innovative methods.[11] Based on the mentioned features, ZnO nanostructures are among the highly investigated material towards efficient photocatalytic degradation of different dyes.[11,22,23] For example, complex shaped ZnO nanostructures made out of one dimensional rods are very advantageous as they exhibit minimum agglomeration and also offer high accessible surface area.[22] Furthermore, due to their hexagonal-wurtzite crystal structure, ZnO nanostructures exhibit several surface facets which contribute towards photocatalytic response.[22,24] The capabilities of ZnO nanostructures for treating different pollutants and organic dyes have been investigated. The involved photocatalytic mechanisms are carefully studied and understood.[4] Additionally, versatility of nanostructuring by simple approaches, such as flame transport synthesis,[25] and many others, opens scope of ZnO nanostructures towards commercial water purification and photocatalysis related applications.

Various nanostructures from ZnO , such as nanowires, nanotubes, nanobelts, etc. have been investigated towards photocatalytic response and the fundamental understandings indicate that surface is the most important parameter contributing to photocatalytic response.[26] Higher the surface area, better the photocatalytic response, including an additional contribution from crystalline facets.[22,26–28] Measuring

the overall surface accessible for photocatalytic activity is challenging as the agglomeration of nanoparticle powder in dispersion cannot be neglected and this requires uniform nanostructures. Additionally, the contribution of nanostructures on photocatalytic dye degradation has been investigated, except fewer studies exist of the impact of photocatalytic experiment on the surface of the involved nanostructures. The effects of the dye on the surface of these nanoscale materials would be a very important information for the broad photocatalysis community. Realizing the importance of these aspects, a compatible nanostructural ZnO was selected, i.e., ultralong (up to several millimeters long) ZnO micro- and nanowire for photocatalytic investigations against methylene blue (MB) dye degradation. These micro- and nano ZnO wires can easily be tracked before and after photocatalytic treatments and their surface modifications after a PC process can be monitored with SEM. In the present work, ZnO micro- and nanowires synthesized by FTS process were used to study the photocatalytic degradation of methylene blue. The observations suggest that microscopic structural pattern on the microwire surface exhibit higher catalytic activity (of ~ 5.2 times) in contrast to ZnO thin films. Multiple photocatalytic cycles forms crease patterns on the microwires, effects of these patterns on the photocatalytic property of the wires. SEM, Raman and X-ray photoelectron spectroscopies, etc. were employed to study the microwires before and after photocatalysis. The photocatalytic results have been carefully presented and discussed including possible MB decomposition pathways.

2. Materials and Methods

2.1 Synthesis of ultralong ZnO micro- and nanowires

For the synthesis of the ultralong ZnO micro- and nanowires, a modified strategy of flame transport synthesis (FTS) method[25] was followed. As contrast to a muffle furnace, a furnace with gas inlets for N₂ and pressured air (flow rate controlled by flowmeters) was utilized in modified FTS approach as shown in **Figure 1a**. A metallic precursor - Zn wire (bought from Alfa Aesar GmbH & CoKG, Germany) – was placed in a metallic/ceramic crucible (the geometry of the wire is presented in the **Figure 1a(i)**). The crucible was covered by a hollow ceramic cylinder with both open ends (**Figure 1b**). A couple ceramic stripes were placed on top of the ceramic cylinder to limit the oxygen turbulence flow during the growth process (the synthesis setup is shown in the **Figure 1b**). The furnace (supplied by Teyfel GmbH, Germany) was preheated to 800 °C (in ambient oxygen atmosphere) and the crucible with the Zn precursor was inserted into the oven. The furnace was rapidly heated to 950 °C (with ramp rate of 25 °C/min), which was maintained for 15 minutes. During the process, additional source for pressured air was provided at a flowrate of 0.68 l/min. After the process, the furnace was left to naturally cool down and ZnO micro- and nanoscale wires grown (appears as white grass) over the edges of the crucible as well as over the ceramic stripes can be seen in **Figure 1b**.

2.3. Morphological and surface characterization

Morphology of the grown ZnO micro- and nanowires was studied using scanning electron microscopy (SEM) and energy-dispersive X-ray spectroscopy (EDS) (ZEISS Ultra Plus microscope, Kiel, Germany) with a field emission gun, operated at 8 kV for SEM imaging and at 20 kV for EDS characterization. For chemical analysis of the ZnO micro- and nanowire- were performed by Raman spectroscopy under ambient condition using WITec alpha300 RA, with a triple grating spectrometer (grating parameters were 600 g/mm BLZ = 500NM) and a CCD detector. A green laser (excitation wavelength of 532.2 nm) was used. Spot size on the sample was of ~ 1.41 μm and maximum power at the sample surface was ~ 52 mW. The scattered beam was collected by an optical fiber (diameter of 50 μm). Obtained data was analyzed using a WITec Project manager. The X-ray photoelectron spectroscopy (XPS, Omicron Nanotechnology GmbH) was utilized for

surface characterization of the ZnO micro- and nanowires. The XPS measurements were performed on the ZnO microwires before and after the photocatalytic experiments and no ion beam treatment (surface cleaning) was applied prior to XPS analysis. The obtained spectra were charge referenced using aliphatic carbon at the binding energy of 285.0 eV.[29] The survey and high-resolution spectra were measured with pass energies of 100 eV and 30 eV, respectively.

2.4 Photocatalytic response measurements

For the evaluation of the photocatalytic activity, a setup described in a previously published work[30] was utilized, with a LED-based UV-source having a wavelength maximum at 365 nm (peak width measured to be of ~20 nm). The UV-light intensity at the cuvette's surface was measured to be ~0.35 mW/cm². A quartz cuvette (all five inner sides polished) holding a 2.5 μM aqueous solution of methylene blue and the sample in a sample holder was placed into the setup, which was equipped with an illumination opening (for UV light), spectrometer and a detector were passing and collecting the signal from the unilluminated areas. The solution was stirred for the whole duration of the measurement. The spectra were collected at every 5 min in a spectral range of 200-1000 nm using StellarNet EPP2000C-SR-50 spectrophotometer (with SL5-DH light source). Prior to each PC-experiment ZnO structures were immersed into the MB solution and kept there under continues stirring for 20 minutes to rule out possible errors through sorption of MB molecules onto the ZnO surface. After that, UV source was switched on and data collection started. For monitoring the impact of MB absorption onto ZnO the measurement without prior immersion and without UV illumination was carried out. Based on that, a time of 20 minutes was chosen to wait for in all further PC experiments involving ZnO structures and MB solution. MB stability under UV illumination was checked as well (**Figure S1**). The decrease in the measured peak intensity (specific for MB) under these conditions was about 0.04 in terms of relative absorbed intensity. Furthermore, in the subsequent PC experiments with ZnO structures involved the decrease of relative absorbed intensity was of 0.27; 0.5 and 0.96. Thus, the slight change in the MB concentration under UV illumination was considered as of least importance.

2.5 Local pH measurements

The pH values in the electrolyte were measured 40 μm from the surface of the ZnO needles embedded in the polythiourethane (PTU) matrix. PTU purchased from Fluid-& Prozesstechnik GmbH (Waltershausen, Germany) is a two component thermoset, chemically inert after curing. After mixing the two components, hexamethylene diisocyanate (HDI) and pentaerythritol tetrakis(3-mercaptopropionate) (PETMP) at a weight ratio of 1.4:1, the mixture was poured into a cylindrical mould with a diameter of 30 mm and 20 mm in depth. This mixture was then allowed to cure. ZnO needles were dropped after 20 minutes of curing on to the surface of the partially cured PTU to avoid sinking of the needles. The sample was then place in a furnace at 80 °C overnight for complete curing. Top layer of the sample was sanded to remove the polymer coating and to expose the ZnO surface. The PTU holder under stagnant conditions with a commercial scanning ion-selective electrode technique (SIET) equipment from Applicable Electronics, which was controlled by LV4 software from Science Wares. The local pH was mapped using a glass-capillary microelectrode with a tip orifice diameter of 1.8±0.2 μm. Glass-capillaries were back-filled with an inner reference solution (0.01 M KH₂PO₄+0.1 M KCl) and tip-filled with a H⁺-selective membrane cocktail based on tridodecylamine (Fluka, Ref. 95293, Sigma Aldrich, Germany). A homemade Ag/AgCl/0.1 M KCl, 0.01 M KH₂PO₄ electrode was used as the external reference electrode. A point by point, move - wait (0.6 s) - measure (0.8 s) scheme took approximately 40 min to complete a 400-points line scan. More details of the experimental setup can be found elsewhere.[31]

3. Results and Discussion

3.1 Growth of ultralong ZnO micro- and nanowires

The FTS growth process works on the principle of solid vapor solid growth from Zn vapor and ambient oxygen into the flame (converts metallic Zn microparticles/wire into vapor phase) inside the oven. If there is no catcher substrate, the normal nucleation and growth process leads to formation of tetrapodal shaped particles. However, if there is any defect site available, it works as a favorable nucleation center leading to prominent 1D nanostructure growth.[11,25,32] The applied catcher substrate in the present work offers many defect sites which facilitate 1D ZnO nanowire growth in the FTS process. The nanowire dimensions (diameter, length) are mainly influenced by the existing precursor material which is relatively high in present case and hence growth of ultralong ZnO micro- and nanowires with length scales of nearly up to 1.5 cm can be grown as shown by SEM image in **Figure 1c**. A big piece with several ZnO wires was harvested and analyzed in SEM which confirmed the interconnected tetrapodal networks as the base (**Figure 1d**). The long ZnO micro- and nanowires (**Figure 1c**) exhibit hexagonally faceted morphologies (**Figure 1e**). The SEM analysis (**Figure 1c**) reveals that the cross-section of the grown ZnO micro- and nanowires range from 200 nm to 7 μm and their lengths range from hundreds of micrometers to several millimeters with very high aspect ratio of $\sim 1:1000$. The growing procedure of the modified-FTS process was investigated by SEM which suggests that it follows a two-step growth process. On the defect sites offered by the catcher substrate, initially a ZnO network is grown which then serves as bed for the growth of long ZnO micro- and nanowires. The most outstanding aspect of presently adopted synthesis is not only the rapid and homogeneous growth of the ZnO micro- and nanowires but also the fact that these ZnO micro- and nanowires are firmly attached to the underneath ZnO bed, making their utilizations even easier, as there is no need to use any outside substrate for the wire's growth, which were directly used here also without any further modification.

3.3. Photocatalytic degradation response

MB decomposition process

ZnO nanostructures, in general, exhibit good photodegradation capabilities against methylene blue.[1,4,6] The involved photocatalytic degradation paths and results corresponding to grown ZnO micro- and nanowires with respect to MB are briefly presented in **Figure 2**. The mechanistic insights about the MB decomposition process under the attachment of $\text{OH}\cdot$ radical attacks and aromatic central ring protonation (by H^+ and/or free electrons) are given in **Figure 2a** and corresponding photodegradation mechanism by ZnO micro- and nanowires under UV illumination (**Figure 2b**). During the photocatalysis study, the UV-visible spectra was recorded at every 5 min intervals under UV light on and off conditions (**Figure 2d-e**) which is plotted in **Figure 2c**. The intensity of the absorption peak at 664 nm (reported as the MB characteristic peak) was monitored throughout the PC process and is plotted versus the time of the reaction (**Figure 2c**). It can be clearly observed that the photodegradation mechanism occurs much faster under the UV light ON condition in concurrence with from literature studies on ZnO based MB degradation.[33] It is very obvious from the shown result that without UV-irradiation, the MB degradation response from the ZnO micro- and nanowires is quite negligible (**Figure 2a**). Several literature studies suggest that the presence of the $\text{OH}\cdot$ radicals are the most necessary elements towards the degradation of MB molecules.[34–38] The $\text{OH}\cdot$ radicals are formed at the surface of ZnO micro- and nanowires when illuminated with UV light of $\lambda \leq 367.9$ nm (larger than ZnO bandgap energy[23]) resulting in the creation of electron-hole pairs. The absorbed oxygen species and OH^- ions react with the photogenerated carriers leading to the formation of and $\text{OH}\cdot$ radicals.[22,35] The Fourier transform infrared spectroscopy studies from existing literature suggest that

during decomposition pathways the side chains of MB are attacked by $\text{OH}\cdot$ radicals which leads to demethylation process.[34,36] The literature works suggest that the color change in MB contributes to the protonation in the aromatic ring H^+ or photogenerated holes and it is most likely reversible reaction process[36,39–41] but it is still an open question being actively discussed.

3.4 Self-nanostructuring: Effect of photocatalyst on ZnO micro- and nanowires

Morphological evolutions

The literature suggests that all the nanomaterials based photocatalytic research works have been nicely reported and discussed about the response of involved nanomaterials towards photocatalytic degradation of dyes under UV illumination. However, the effect of photocatalytic dye-based solutions under UV illumination over the involved nanoparticles cannot be completely ignored as in nanoscale dimensions their surfaces are very sensitive to any surrounding disturbances, especially if it is in a wet chemical form. The FTS synthesized ZnO micro- and nanowires (reference samples) were repeatedly treated with MB photocatalytic process and after several cycles a visual change in the color was realized which motivated us to investigate more in this direction. The ZnO micro- and nanowire samples (after 1, 2 and 4 cycles) were investigated in SEM in detail which confirmed formation of rippled type pattern (concentric rings) at the entire surface as shown by SEM images in **Figure 3a-f**. It can be clearly observed that with increasing number of MB exposure cycles, the ripple shaped structures got prominent (**Figure 3a-f**) which is most likely due to the dissolution of Zn^{2+} and O^{2-} ions from the surface in MB solution (under UV-light exposure). Additionally, the rippled structure might be an indication of certain planes, that are perpendicular to the c-axis, to be more dissolved in a PC process than the others. Such behavior of single-crystalline ZnO structures has been observed and confirmed in the studies on preferential wet-chemical etching.[42] Depending on utilized etchants the polar planes ((10-11) and (000-1), consisting of oxygen ions) were selectively removed or stayed intact, respectively. Thus, the MB exposures induce a nanostructuring phenomenon at the surface of ZnO micro- and nanowires and these ripples shaped etched nanostructures (**Figure 3a-f**) increases the overall surface contributions which is accessible to MB. Analogous structures, built up of several planes of ZnO being stuck on top of each other, have been tested for the photodecomposition of the volatile organic compounds and have demonstrated an outstanding performance.[43] In a similar way, in present study as a consequence of increased surface area, the photocatalytic response against methylene blue was enhanced as shown in **Figure 4a-e**. For the ZnO microwires in the second PC cycle the measured absorbed intensity of MB characteristic peak went below 10% of the starting intensity after 90 minutes. This decrease is clearly visible from the spectral dependency of the absorbed intensity around 664 nm in **Figure 4e**. In order to understand the MB induced nanostructuring behavior, another sample of the ZnO micro- and nanowires was immersed into MB (1, 2 and 4 photocatalytic cycles for 2, 4 and 6 hours, respectively) without any UV illumination (**Figure S2**). It was observed that in the absence of UV illumination, no surface nanostructuring occurs as confirmed by SEM images (shown in Supporting Information **Figure S2**). Thus, the SEM investigations suggest that MB as such exhibits no role towards surface nanostructuring in ZnO micro- and nanowires but in combination with UV illumination, it has an effect towards interesting surface restructuring which has been investigated in detail here using different characterizations as reported in the following sections.

3.5. XPS analysis

The XPS studies were performed on reference ZnO micro- and nanowires and after two cycles of methylene blue decomposition. Corresponding survey spectra of both specimens are presented in the **Figure 5a**, including peak assignments and elemental compositions. It can be clearly seen that only Carbon, Oxygen and Zinc elements were detected, with relatively high concentration of carbon (~11 at% for reference sample), which could be referred to surface contamination in the ambient atmosphere.[29] Noticeably, the original ZnO micro- and nanowires are oxygen deficient with Zn:O ratio of around 1:0.54, while after two MB decomposition cycles the Zn:O ratio has improved significantly (Zn:O~1:0.64) hinting towards the Zn oxidation in MB solution (See **Table I**). Two mechanism can be responsible, either, that after MB reaction (under UV illumination) some of the surface Zn^{2+} ions were photoetched and crystal stoichiometry was slightly changed or that the adsorbed oxygen species from the reaction solution contributed to the total increase in the oxygen content after the photocatalytic reaction. Furthermore, the amount of carbon has increased after photocatalytic measurements, which is most likely related to extra carbon adsorption during MB decomposition. C-1s high resolution spectra including deconvolution for both samples (before and after MB experiment under UV-light on condition) are shown in Supplementary **Figure S3 a, c**. The aliphatic carbon at 285.0 eV is the main component in these spectra, however, the additional carbon oxides (C-O, 286.8 eV; C=O, 288.9 eV) or hydroxide groups were also detected on the surface.

The high resolution XPS measurements (**Figure 5 b,c**) conducted on the oxygen peak revealed several distinctive characteristics. The deconvolution was done with three components denoted as O_I , O_{II} and O_{III} . The main peak O_I has a binding energy of 530.5 eV and has been assigned to the O^{2-} anions in the wurtzite structure of ZnO.[44,45] The envelope form of the oxygen peaks (shown in the **Figure 5b-c**) suggest the presence of the peaks O_{II} and O_{III} with slightly higher binding energies. As described in literature, these peaks originate from O^{2-} crystal ions in an oxygen-deficient surrounding[45–47] and from OH^- (531.09 eV) or O_2 (533.0 eV) species adhered at the crystal's surface.[44–46] Based on the fitting of the O-1s for pristine ZnO and ZnO after MB reaction (under UV illumination), the approximate amounts of O_I , O_{II} and O_{III} were determined (given in **Table II**). The obvious conclusion from these calculations is that the ratio of the lattice oxygen atoms (O_I signal) to the loosely bound oxygen and OH^- or O_2^{2-} species ($O_{II}+O_{III}$) is 1:0.40 (untreated ZnO) and 1:0.68 (ZnO after 2 MB cycles). This again confirmed the slightly increased amount of other oxygen species which have originated after the MB decomposition reactions at the surface of ZnO micro- and nanowires. Additionally, the increased amounts of O_{II} species (loosely bound oxygen ions) is ~ 27.6% after MB-treatment as compared to ~18.2% for untreated sample pointing towards a possible alterations in the crystal structure of ZnO micro- and nanowires after the photocatalysis process (under UV illumination). The comparison (overlap) of two oxygen peaks for treated and untreated ZnO is presented in the **Figure S3b**, along with the Zn-2p doublet spectra (**Figure S3d**), once more illustrating the enhanced oxidation after MB experiment which supports the formation of wrinkled nanostructures at the surface as shown in **Figure 3**.

3.6. Raman spectroscopy studies

The photodegradation process of methylene blue very likely occurs simultaneous to the dissolution of ZnO surface. The possible compositional changes in the ZnO micro- and nanowires after a PC cycle were tracked via Raman spectroscopy studies. Scans in the **Figure 6a & 6b** display surface scans of a reference ZnO microwire and a microwire after two PC cycles. The spectral scans were generated by using the filter of 100-600 cm^{-1} (in this spectral range characteristic peaks of ZnO are the most intensive). These scans show several

inhomogeneities in ZnO peak intensities in case of treated ZnO microwires. Both, the treated and untreated ZnO micro- and nanowires samples exhibit the typical peaks for wurtzite crystal structure of ZnO in the recorded spectra. All the Raman peaks, described in literature[48] (E_2^1 ,low; E_2^2 - E_2^1 ; E_2^2 ,high; A_1 (TO); E_1 (LO)) were identified (**Figure 6c,d**) in the obtained spectra. A broad peak at 2750-2800 cm^{-1} was additionally observed for the treated ZnO micro- and nanowires, which could be assigned to the organic residue on the surface of the ZnO after the photocatalysis (SEM image in Supporting Information, **Figure S4**). Anyhow, almost no traces of OH^- ions were observed in the Raman spectrum corresponding to treated ZnO micro- and nanowires (with MB under UV illumination). The single spectrum taken from the green marked points in the surface scans from treated and untreated micro- and nanowires reveals a noticeable difference in the E_2^2 (high) peak. The E_2^2 high peak is known to indicate the crystalline quality of the ZnO wurtzite structure. The treated ZnO micro- and nanowires show a considerable decrease in E_2^2 high peak's intensity, indicating an increased lattice disorder at the surface. Considering the wavenumber region from 520 to 650 cm^{-1} , the peaks A_1 (LO) and E_1 (LO), known for the oxygen disorder in the lattice, are more vividly present for the treated ZnO micro- and nanowires. Thus, an increase in the Raman bands are most likely due to the oxygen disorder, and an indication of distorted crystallinity (E_2^2 high decrease) in the ZnO micro- and nanowires after several cycles of MB decompositions (under UV illumination on condition) and both altogether confirm the occurrence of structural changes at the surface of the ZnO micro- and nanowires. The SEM, XPS and Raman spectroscopy results altogether indicate a surface nanostructuring of ZnO micro- and nanowires during photocatalytic treatments under UV illumination.

3.7. pH-mappings of ZnO treated MB solutions

The photocatalysis mainly took place at the ZnO micro- and nanowire surface and hence the major involvement of the OH^- ions and their radicalization via photo-created charge carriers at the ZnO surface result in methylene blue undergoing a decomposition reaction. This leads to an unbalance between the H^+ and OH^- amounts in the aqueous medium where the photodecomposition reactions take place and it might instantly influence the pH value of the surroundings regions in the solution. This change in pH values was traced via an *in-situ* measurement setup during an on-going photocatalysis experiment and corresponding results are shown in **Figure 7**. Based on the previously performed EDX analysis, the setup of the wires embedded in PTU (chosen due to its optimal stiffness required for polishing without damaging the immersed structures) with the upper layer being polished, revealing uncovered ZnO surface for the reactions to take place during the pH mapping (**Figure 7a, b**). The maps of local pH distribution were taken in a plane 40 μm from the polished surface of PTU holder incorporating ZnO needles (**Figure 7c**). The pH value of the aqueous electrolyte directly above the ZnO needles was slightly shifted to more alkaline values when the photocatalytic process was activated (**Figure 7d-f**). While the difference between the bulk pH and the highest pH values above ZnO needles was roughly constant during the UV irradiation, 0.23 pH units (**Figure 7d-f**), this difference increased abruptly to 0.42 pH units difference (**Figure 7g**) as soon as the UV-illumination was switched off and then gradually decreased from 0.31 pH units (1.5 hours) to 0.15 pH units after (16.5 hours), **Figures 7 h and i**. The slight differences, compared to bulk pH, visible at the middle right side of the maps (**Figure 7d-i**) might have been originated from the cavity in the polymer mold (bubble artifact happened during the preparation, **Figure 7c**), where the electrolyte could not circulate freely and hence could not immediately accommodate the changes produced through the reactions at the surface of ZnO micro- and nanowire.

3.8. Self-nanostructuring mechanism

The observed nanostructuring phenomenon in ZnO structures by photocatalytic solution under the UV illumination condition is quite interesting and fairly very new. Most of the ZnO nanostructures based photocatalysis works in the literature mainly discussed about the effect of ZnO nanomaterials towards photocatalytic dye degradation rather than vice versa, i.e., not even a single report can be found which talks about the role to photocatalytic solution over nanoparticles, at least to the best of our literature knowledge. However, photocatalytic solution mediated dissolution of quantum dot structures from other semiconductors, such as, CdS, under light illumination has been reported.[49,50] It has been found that the parameters like, semiconducting nature of involved material, light illumination, and the chemical response (electron or hole capturing abilities) of the photocatalytic dye play a very important role. The light illumination (with wavelength in the vicinity of the bandgap) leads to creation of electron-hole pair generation. The surface restructuring phenomenon in CdS quantum dots has been reported in methylviologen solution (organic dye) and light illumination (in the bandgap wavelength region). [49,50] Methylviologen exhibit strong electron acceptor tendency and the light illumination leads to creation of electron-hole pairs in CdS quantum dots. The majority of generated electrons are captured by the methylviologen solution thereby leaving many hole behind which then react with surface atoms of the quantum dots.[49,50] Thus, the excessive holes can then initiate the dissolution of the semiconductor's surface leading to a photocorrosion process up to a great extent. To confirm the role of e-h pairs during the photocatalytic process, the methylviologen (MV²⁺), a commercial dye was added to the solution which served as an electron scavenger preventing the newly created electrons from recombination with holes and this lead to a rapid dissolution.[50] Similar to CdS, ZnO is a direct band gap semiconductor and the involved methylene blue dye is strong electron acceptor hence we strongly believe that electron-hole creation under light illumination is most likely responsible for the observed self-nanostructuring under light illumination condition. The UV light illumination creates e-h pairs in ZnO and even light below bandgap energy can also excite e-h pairs because of interesting surface defects.[51] No change in surface morphology of ZnO micro- and nanowires immersed in methylene blue was observed after several cycles and multiple hours (Supplementary Information, **Figure S2**). The MB molecules in present case of UV illuminated ZnO micro- and nanowires, act as electron scavengers leading to a hole mediated photocorrosion[33] which can be represented by the equation (4):



The photocorrosion behaviors under light illumination have been mainly reported for semiconducting quantum dots[49,50] or nanofilms[33] but considering into account their very nanoscale dimensions, the changes in the size and morphology were quite crucial aspects. In another case, the atomic layer deposited (ALD) ZnO nanofilm was up to 50% destroyed after 24 hours of photocorrosion and thus, the active ZnO nanofilm layer necessary for photocatalytic activity was disrupted and became highly porous.[33] The present observations demonstrate that the surface accessibility plays very important role, towards both, the photocatalytic degradation response against methylene blue (**Figure 4**) as well as self-nanostructuring (**Figure 3**). In the self-nanostructured ZnO micro – and nanowire samples with selectively removed planes along the c-axis, the interchange of MB molecules in the solution is much faster and hence enhanced the overall response. The photocatalytic data of self-nanostructured ZnO micro – and nanowires displayed an enormous improvement in the degradation rate, reaching the values of $k = 0.0215 \pm 8.23 \times 10^{-4} \text{ min}^{-1}$ from the linearly fitted data (**Figure 3, Table III**). With increase in number of photocatalytic cycles under UV illuminated ZnO micro- and nanowires, the self-nanostructuring behavior has become prominent (**Figure 3**) which is in good agreement too as each photocorrosion cycle (due to MB) lead an enhanced surface accessible for MB molecules in subsequent photocatalytic cycles and hence an improved response (**Figure**

3a,b,e, f). Somehow, the prominent difference in the profile C/C_0 for the second and the first PC run could be understood with consideration of photogenerated charge carriers and their behaviour at the ZnO surface. First, during the UV illumination generated charge carriers are trapped at the defect sites in ZnO, where with contribution of MB molecules (from the solution) the surface restructuring occurs. Simultaneously to that, the rest of the photogenerated charge carriers participate in the photocatalytic process at the ZnO surface. As soon as the defect sites are dissolved, the PC process runs more effectively, as more and more of the created free charge carriers can participate in the photocatalysis. The **Table III** compares the rate constants for different samples which indicate the ZnO micro- and nanowires after two decomposition cycles exhibit a maximum rate constant. The linear fitting of the $-\ln(C/C_0)$ was performed based on the Langmuir-Hinshelwood model following a pseudo-first-order kinetics (equation 5):

$$\ln\left(\frac{C_0}{C}\right) = k_{abs} \cdot t \quad (5)$$

The coefficients utilized in the fitting are presented in the **Table IV**. After repeating experiments under identical experimental conditions several times, it has been observed that the photocorrosion starts at certain points on the ZnO facets and defect locations (these flames made ZnO micro- and nanowires exhibit many kinks and edges). The most active surfaces are etched easily and in case of ZnO, it is most likely the (0001) plane but the existing surface defects are also easily locations for the start of the etching process. It is assumed that both of them, the high energy surface facets as well as surface defects in the flame grown ZnO micro- and nanowires are responsible for the observed photocorrosion behavior but to exactly confirm this, advance studies based on in-situ TEM and chemistry techniques under optimal experimental conditions would be necessary.

4. Conclusions

Photocatalysis using compact micro- and nanostructures from semiconductors under harsh conditions is a very intriguing research topic for relevant chemical purifications. In the present work, the single crystalline ZnO micro- and nanowires were efficiently synthesized and characterized via SEM and Raman spectroscopy investigations. In order to study the role of overall surface area and geometry, the ZnO micro- and nanowires were compared to a 2D ZnO substrate. The photocatalytic response from the ZnO micro- and nanowires and the 2D ZnO against methylene blue decomposition was analyzed. Comparison showed that the pristine ZnO micro- and nanowires exhibit better performance. It is observed that the PC effect is strongly influenced by UV light irradiation, which results in much better performance. Additionally, a photocorrosion mediated self-nanostructuring behavior of the ZnO micro- and nanowire surface was observed after photocatalytic cycling under UV illumination. The UV induced electron-hole creation and the strong electron capturing capabilities of MB lead the photocorrosion process on the surface of the ZnO micro- and nanowires. Both, the PC degradation and photocorrosion depend on the accessible surface and are complementary to each other. Each photocatalytic cycle resulted in overall increased accessible surface which lead to enhanced photocorrosion and after several cycles a significant improvement in both responses is observed. The SEM, Raman spectroscopy and XPS studies confirmed the self-structuring in ZnO micro- and nanowires due to photocatalytic cycling and the in-situ pH mapping analysis showed an instantaneous change in pH value in the areas surroundings the wires. The presented interplay of photocatalysis and photocorrosion processes in ZnO microwires during the degradation of methylene blue under UV illumination would be of high interest for metal oxide based photocatalytic water purification.

Author Contributions

The manuscript was written through contributions of all authors. All authors have given approval to the final version of the manuscript.

Acknowledgements

This work was financially supported by German Research Foundation within the projects SFB 677 C-14.

REFERENCES

- [1] J. Kou, C. Lu, J. Wang, Y. Chen, Z. Xu, R.S. Varma, Selectivity Enhancement in Heterogeneous Photocatalytic Transformations, *Chem. Rev.* 117 (2017) 1445–1514. doi:10.1021/acs.chemrev.6b00396.
- [2] M.B. Gawande, A. Goswami, F.-X. Felpin, T. Asefa, X. Huang, R. Silva, X. Zou, R. Zboril, R.S. Varma, Cu and Cu-Based Nanoparticles: Synthesis and Applications in Catalysis, *Chem. Rev.* 116 (2016) 3722–3811. doi:10.1021/acs.chemrev.5b00482.
- [3] A.L. Linsebigler, G. Lu, J.T. Yates, Photocatalysis on TiO₂ Surfaces: Principles, Mechanisms, and Selected Results, *Chem. Rev.* 95 (1995) 735–758. doi:10.1021/cr00035a013.
- [4] K.M. Lee, C.W. Lai, K.S. Ngai, J.C. Juan, Recent developments of zinc oxide based photocatalyst in water treatment technology: A review, *Water Res.* 88 (2016) 428–448. doi:10.1016/j.watres.2015.09.045.
- [5] L.K. Adams, D.Y. Lyon, P.J.J. Alvarez, Comparative eco-toxicity of nanoscale TiO₂, SiO₂, and ZnO water suspensions, *Water Res.* 40 (2006) 3527–3532. doi:10.1016/j.watres.2006.08.004.
- [6] L. V. Trandafilović, D.J. Jovanović, X. Zhang, S. Ptasińska, M.D. Dramićanin, Enhanced photocatalytic degradation of methylene blue and methyl orange by ZnO:Eu nanoparticles, *Appl. Catal. B Environ.* 203 (2017) 740–752. doi:10.1016/j.apcatb.2016.10.063.
- [7] M. Kwiatkowski, R. Chassagnon, O. Heintz, N. Geoffroy, M. Skompska, I. Bezverkhy, Improvement of photocatalytic and photoelectrochemical activity of ZnO/TiO₂core/shell system through additional calcination: Insight into the mechanism, *Appl. Catal. B Environ.* 204 (2017) 200–208. doi:10.1016/j.apcatb.2016.11.030.
- [8] C. Santhosh, V. Velmurugan, G. Jacob, S.K. Jeong, A.N. Grace, A. Bhatnagar, Role of nanomaterials in water treatment applications: A review, *Chem. Eng. J.* 306 (2016) 1116–1137. doi:10.1016/j.cej.2016.08.053.
- [9] A. Bhatnagar, M. Sillanpää, Utilization of agro-industrial and municipal waste materials as potential adsorbents for water treatment-A review, *Chem. Eng. J.* 157 (2010) 277–296. doi:10.1016/j.cej.2010.01.007.
- [10] M. Sharma, M. Joshi, S. Nigam, S. Shree, D.K. Avasthi, R. Adelung, S.K. Srivastava, Y. Kumar Mishra, ZnO tetrapods and activated carbon based hybrid composite: Adsorbents for enhanced decontamination of hexavalent chromium from aqueous solution, *Chem. Eng. J.* 358 (2019) 540–551. doi:10.1016/j.cej.2018.10.031.
- [11] Y.K. Mishra, R. Adelung, ZnO tetrapod materials for functional applications, *Mater. Today.* 21 (2018) pp 631–651. doi:10.1016/j.mattod.2017.11.003.
- [12] T. Hrkac, C. Röhl, R. Podschun, V. Zaporozhchenko, T. Strunskus, H. Papavlassopoulos, D. Garbe-Schönberg, F. Faupel, Huge increase of therapeutic window at a bioactive silver/titania nanocomposite coating surface compared to solution, *Mater. Sci. Eng. C.* 33 (2013) 2367–2375. doi:10.1016/j.msec.2013.01.069.
- [13] D.M. Mitrano, E. Rimmele, A. Wichser, R. Erni, M. Height, B. Nowack, Presence of Nanoparticles in Wash Water from Conventional Silver and Nano-silver Textiles, *ACS Nano.* 8 (2014) 7208–7219. doi:10.1021/nn502228w.
- [14] A. Mills, S. Le Hunte, An overview of semiconductor photocatalysis, *J. Photochem. Photobiol. A Chem.* 108 (1997) 1–35. doi:10.1016/S1010-6030(97)00118-4.
- [15] A. Mills, R.H. Davies, D. Worsley, Water purification by semiconductor photocatalysis, *Chem. Soc. Rev.* 22 (1982) 417–425. doi:10.1039/CS9932200417.
- [16] J. Zhao, Y. Kang, S. Neretina, T.B. Demille, R.A. Hughes, A.S. Preston, R. Adelung, Y.K. Mishra, Light-

Mediated Growth of Noble Metal Nanostructures (Au, Ag, Cu, Pt, Pd, Ru, Ir, Rh) From Micro- and Nanoscale ZnO Tetrapodal Backbones, *Front. Chem. | Wwww.Frontiersin.Org.* 6 (2018) 411. doi:10.3389/fchem.2018.00411.

- [17] R. Asahi, T. Morikawa, T. Ohwaki, K. Aoki, Y. Taga, Visible-light photocatalysis in nitrogen-doped titanium oxides., *Science.* 293 (2001) 269–71. doi:10.1126/science.1061051.
- [18] A.L. Linsebigler, G. Lu, J.T. Yates, Photocatalysis on TiO₂ Surfaces: Principles, Mechanisms, and Selected Results, *Chem. Rev.* 95 (1995) 735–758. doi:10.1021/cr00035a013.
- [19] H. Dong, G. Zeng, L. Tang, C. Fan, C. Zhang, X. He, Y. He, An overview on limitations of TiO₂-based particles for photocatalytic degradation of organic pollutants and the corresponding countermeasures, *Water Res.* 79 (2015) 128–146. doi:10.1016/j.watres.2015.04.038.
- [20] A.B. Djurišić, Y.H. Leung, K.H. Tam, Y.F. Hsu, L. Ding, W.K. Ge, Y.C. Zhong, K.S. Wong, W.K. Chan, H.L. Tam, K.W. Cheah, W.M. Kwok, D.L. Phillips, Defect emissions in ZnO nanostructures, *Nanotechnology.* 18 (2007) 95702. doi:10.1088/0957-4484/18/9/095702 M4 - Citavi.
- [21] S.J. Park, G.S. Das, F. Schütt, R. Adelung, Y.K. Mishra, K.M. Tripathi, T. Kim, Visible-light photocatalysis by carbon- nano-onion-functionalized ZnO tetrapods : degradation of 2, 4-dinitrophenol and a plant-model-based ecological assessment, *NPG Asia Mater.* 11 (2019) 8. doi:10.1038/s41427-019-0107-0.
- [22] Y.K. Mishra, G. Modi, V. Cretu, V. Postica, O. Lupan, T. Reimer, I. Paulowicz, V. Hrkac, W. Benecke, L. Kienle, R. Adelung, Direct Growth of Freestanding ZnO Tetrapod Networks for Multifunctional Applications in Photocatalysis, UV Photodetection, and Gas Sensing, *ACS Appl. Mater. Interfaces.* 7 (2015) 14303–14316. doi:10.1021/acsami.5b02816.
- [23] Z.L. Wang, Nanostructures of zinc oxide, *Mater. Today.* 7 (2004) 26–33. doi:10.1016/S1369-7021(04)00286-X.
- [24] A. McLaren, T. Valdes-Solis, G. Li, S.C. Tsang, Shape and Size Effects of ZnO Nanocrystals on Photocatalytic Activity, *J. Am. Chem. Soc.* 131 (2009) 12540–12541. doi:10.1021/ja9052703.
- [25] Y.K. Mishra, S. Kaps, A. Schuchardt, I. Paulowicz, X. Jin, D. Gedamu, S. Freitag, M. Claus, S. Wille, A. Kovalev, S.N. Gorb, R. Adelung, Fabrication of Macroscopically Flexible and Highly Porous 3D Semiconductor Networks from Interpenetrating Nanostructures by a Simple Flame Transport Approach, *Part. Part. Syst. Charact.* 30 (2013) 775–783. doi:10.1002/ppsc.201300197.
- [26] T. Reimer, I. Paulowicz, R. Röder, S. Kaps, O. Lupan, S. Chemnitz, W. Benecke, C. Ronning, R. Adelung, Y.K. Mishra, Single Step Integration of ZnO Nano- and Microneedles in Si Trenches by Novel Flame Transport Approach: Whispering Gallery Modes and Photocatalytic Properties, *ACS Appl. Mater. Interfaces.* 6 (2014) 7806. doi:10.1021/am5010877.
- [27] F. Liu, Y.H. Leung, A.B. Djurišić, A.M.C. Ng, W.K. Chan, K.L. Ng, K.S. Wong, C. Liao, K. Shih, C. Surya, Effect of plasma treatment on native defects and photocatalytic activities of zinc oxide tetrapods, *J. Phys. Chem. C.* 118 (2014) 22760–22767.
- [28] F. Xu, Y. Shen, L. Sun, H. Zeng, Y. Lu, Enhanced photocatalytic activity of hierarchical ZnO nanoplate-nanowire architecture as environmentally safe and facilely recyclable photocatalyst, *Nanoscale.* 3 (2011) 5020. doi:10.1039/c1nr11033k.
- [29] G. Greczynski, L. Hultman, C 1s Peak of Adventitious Carbon Aligns to the Vacuum Level: Dire Consequences for Material's Bonding Assignment by Photoelectron Spectroscopy, *ChemPhysChem.* 18 (2017) 1507–1512. doi:10.1002/cphc.201700126.
- [30] B. Henkel, T. Neubert, S. Zabel, C. Lamprecht, C. Selhuber-Unkel, K. Rätzke, T. Strunskus, M. Vergöhl, F. Faupel, Photocatalytic properties of titania thin films prepared by sputtering versus evaporation and aging of induced oxygen vacancy defects, *Appl. Catal. B Environ.* 180 (2016) 362–371. doi:10.1016/j.apcatb.2015.06.041.
- [31] S. V. Lamaka, J. Gonzalez, D. Mei, F. Feyerabend, R. Willumeit-Römer, M.L. Zheludkevich, Local pH and Its Evolution Near Mg Alloy Surfaces Exposed to Simulated Body Fluids, *Adv. Mater. Interfaces.* 5 (2018) 1800169. doi:10.1002/admi.201800169.
- [32] N. Faraji, C. Ulrich, N. Wolff, L. Kienle, R. Adelung, Y.K. Mishra, J. Seidel, Visible-Light Driven Nanoscale Photoconductivity of Grain Boundaries in Self-Supported ZnO Nano- and Microstructured Platelets, *Adv. Electron. Mater.* 2 (2016) 1600138. doi:10.1002/aelm.201600138.

- [33] Y.-Q. Cao, J. Chen, H. Zhou, L. Zhu, X. Li, Z.-Y. Cao, D. Wu, A.-D. Li, Photocatalytic activity and photocorrosion of atomic layer deposited ZnO ultrathin films for the degradation of methylene blue., *Nanotechnology*. 26 (2015) 024002. doi:10.1088/0957-4484/26/2/024002.
- [34] C. Yang, W. Dong, G. Cui, Y. Zhao, X. Shi, X. Xia, B. Tang, W. Wang, Highly efficient photocatalytic degradation of methylene blue by P2ABSA-modified TiO₂ nanocomposite due to the photosensitization synergetic effect of TiO₂ and P2ABSA, *RSC Adv.* 7 (2017) 23699–23708. doi:10.1039/C7RA02423A.
- [35] Y. Nosaka, A. Nosaka, Understanding Hydroxyl Radical (\bullet OH) Generation Processes in Photocatalysis, *ACS Energy Lett.* 1 (2016) 356–359. doi:10.1021/acsenerylett.6b00174.
- [36] Z. Yu, S.S.C. Chuang, Probing methylene blue photocatalytic degradation by adsorbed ethanol with in situ IR, *J. Phys. Chem. C*. 111 (2007) 13813–13820. doi:10.1021/jp0715474.
- [37] J. Qin, X. Zhang, C. Yang, M. Cao, M. Ma, R. Liu, ZnO microspheres-reduced graphene oxide nanocomposite for photocatalytic degradation of methylene blue dye, *Appl. Surf. Sci.* 392 (2017) 196–203. doi:10.1016/J.APSUSC.2016.09.043.
- [38] J. Wang, T. Tsuzuki, L. Sun, X. Wang, Reducing the Photocatalytic Activity of Zinc Oxide Quantum Dots by Surface Modification, *J. Am. Ceram. Soc.* 92 (2009) 2083–2088. doi:10.1111/j.1551-2916.2009.03142.x.
- [39] S. Sohrabnezhad, A. Pourahmad, R. Rakhshae, A. Radaee, S. Heidarian, Catalytic reduction of methylene blue by sulfide ions in the presence of nanoAlMCM-41 material, *Superlattices Microstruct.* 47 (2010) 411–421. doi:10.1016/j.spmi.2009.12.006.
- [40] M.Z. Ghori, S. Veziroglu, B. Henkel, A. Vahl, O. Polonskyi, T. Strunskus, F. Faupel, O.C. Aktas, A comparative study of photocatalysis on highly active columnar TiO₂ nanostructures in-air and in-solution, *Sol. Energy Mater. Sol. Cells.* 178 (2018) 170–178. doi:10.1016/j.solmat.2018.01.019.
- [41] T. Zhang, T. Oyama, A. Aoshima, H. Hidaka, J. Zhao, N. Serpone, Photooxidative N-demethylation of methylene blue in aqueous TiO₂ dispersions under UV irradiation, *J. Photochem. Photobiol. A Chem.* 140 (2001) 163–172. doi:10.1016/S1010-6030(01)00398-7.
- [42] X.G. Han, Y.Q. Jiang, S.F. Xie, Q. Kuang, X. Zhou, D.P. Cai, Z.X. Xie, L.S. Zheng, Control of the surface of ZnO nanostructures by selective wet-chemical etching, *J. Phys. Chem. C*. 114 (2010) 10114–10118. doi:10.1021/jp101284p.
- [43] Z.R. Tian, J.A. Voigt, J. Liu, B. Mckenzie, M.J. Mcdermott, M.A. Rodriguez, H. Konishi, H. Xu, Complex and oriented ZnO nanostructures, *Nat. Mat.* 2 (2003) 821–826.
- [44] H.Y. Lee, B.K. Wu, M.Y. Chern, Study on the formation of zinc peroxide on zinc oxide with hydrogen peroxide treatment using x-ray photoelectron spectroscopy (XPS), *Electron. Mater. Lett.* 10 (2014) 51–55. doi:10.1007/s13391-013-2244-x.
- [45] L.L. Yang, Q.X. Zhao, M. Willander, X.J. Liu, M. Fahlman, J.H. Yang, Origin of the surface recombination centers in ZnO nanorods arrays by X-ray photoelectron spectroscopy, *Appl. Surf. Sci.* 256 (2010) 3592–3597. doi:10.1016/J.APSUSC.2009.12.160.
- [46] W. Khan, F. Khan, H. Ajmal, N. Huda, J. Kim, S.-D. Kim, W. Khan, F. Khan, H.M.S. Ajmal, N.U. Huda, J.H. Kim, S.-D. Kim, Evolution of Structural and Optical Properties of ZnO Nanorods Grown on Vacuum Annealed Seed Crystallites, *Nanomaterials*. 8 (2018) 68. doi:10.3390/nano8020068.
- [47] S.N.Q.A. Abd Aziz, S.-Y. Pung, N.N. Ramli, Z. Lockman, Growth of ZnO nanorods on stainless steel wire using chemical vapour deposition and their photocatalytic activity., *Sci. World J.* 2014 (2014) 252851. doi:10.1155/2014/252851.
- [48] S. Jabri, H. Souissi, A. Souissi, A. Meftah, V. Sallet, A. Lusson, P. Galtier, M. Oueslati, Investigation of the vibrational modes of ZnO grown by MOCVD on different orientation planes, *J. Raman Spectrosc.* 46 (2015) 251–255. doi:10.1002/jrs.4617.
- [49] H. Matsumoto, T. Sakata, H. Mori, H. Yoneyama, Preparation of monodisperse CdS nanocrystals by size selective photocorrosion, *J. Phys. Chem.* 100 (1996) 13781–13785. doi:10.1021/jp960834x.
- [50] A. Van Dijken, A.H. Janssen, M.H.P. Smitsmans, D. Vanmaekelbergh, A. Meijerink, Size-Selective Photoetching of Nanocrystalline Semiconductor Particles, *Chem. Mater.* 10 (1998) 3513–3522. doi:10.1021/cm980715p.
- [51] A. Janotti, C.G. Van de Walle, Fundamentals of Zinc Oxide as a Semiconductor, *Reports Prog. Phys.* 72 (2009) 126501. doi:10.1088/0034-4885/72/12/126501.

FIGURE 1

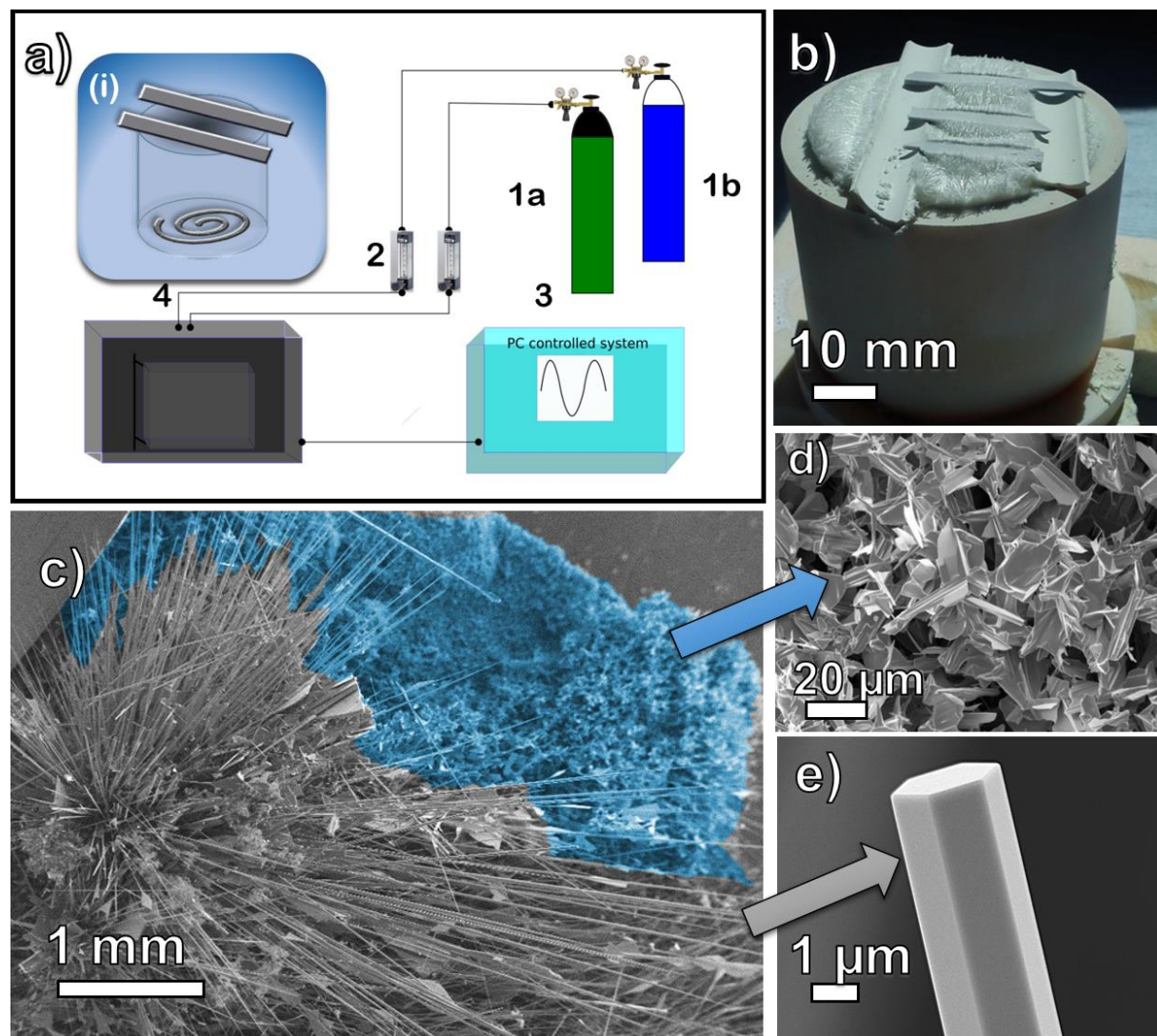


Figure 1. (a) Schematic of the setup for the controlled ZnO growth. (b) A camera image of the working setup after the synthesis took place, where the white wires with a length of several millimeters could be distinguished at the top of the cylinder with bare eyes. (c)-(e) SEM images on the ZnO microstructure synthesis of pristine ZnO wires: (c) a clearly visible substrate beneath the wires (indicated in blue) from which the growth of the ZnO microwires takes place. (d) The substrate is covered with 3D-facets randomly oriented to each other. (e) Distinct hexagonal facets of a single ZnO microwire having a hexagon - shaped cross section.

FIGURE 2

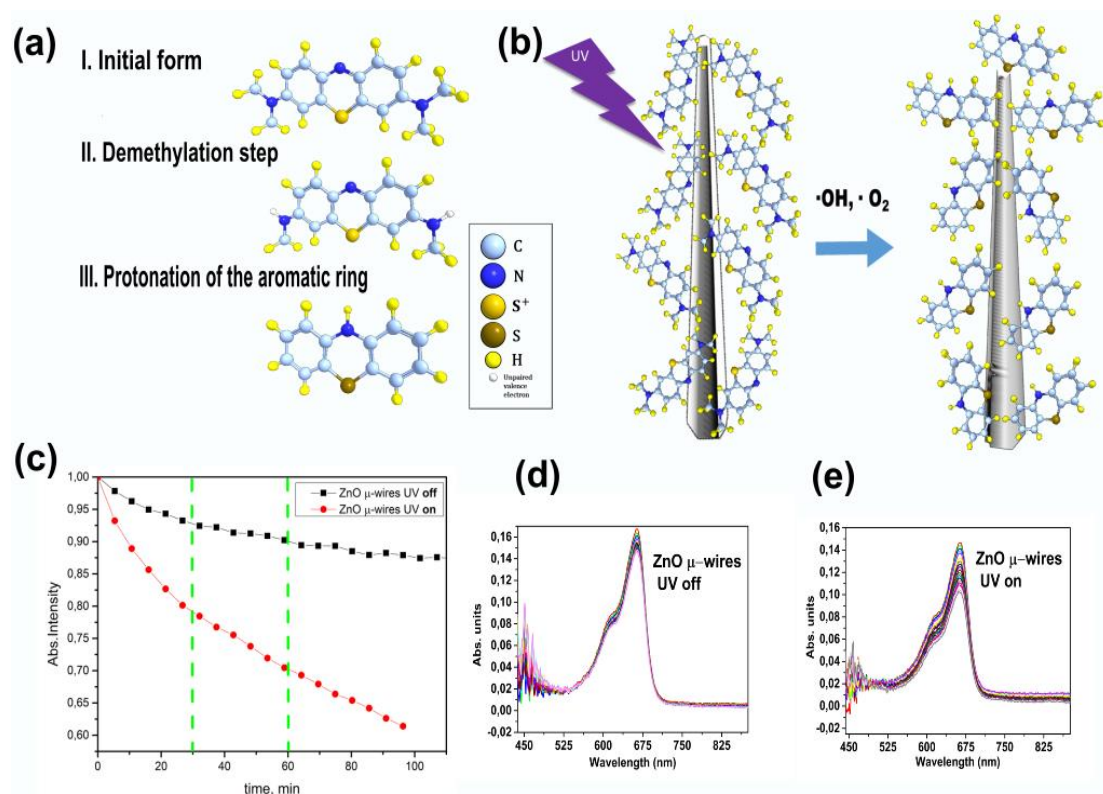


Figure 2. (a) Steps of the MB decay. First the methyl-containing sides are getting attacked by $\text{OH}\cdot$ radicals, leading to a demethylation of the side-chains. This is followed by the protonation of the aromatic central ring via H^+ and/or free electrons. Both processes cause a color change observed during the PC process. (b) A general overview of a ZnO microneedle with adsorbed MB molecules. After UV is switched on, the radicals are formed causing the reactions described in (a). (c) Catalysis comparison of the degradation performance of ZnO microwires (μ -wires) without UV source (black points) and with UV source turned on (red points). Green dotted lines indicate the absorbed intensities at the MB characteristic peak of $\lambda=664.08$ nm at $t_1 = 30$ min and $t_2 = 60$ min. Insets (d) and (e) show the individual spectra taken with UV source off and on, respectively. Each spectrum was taken in 5 min intervals.

FIGURE 3

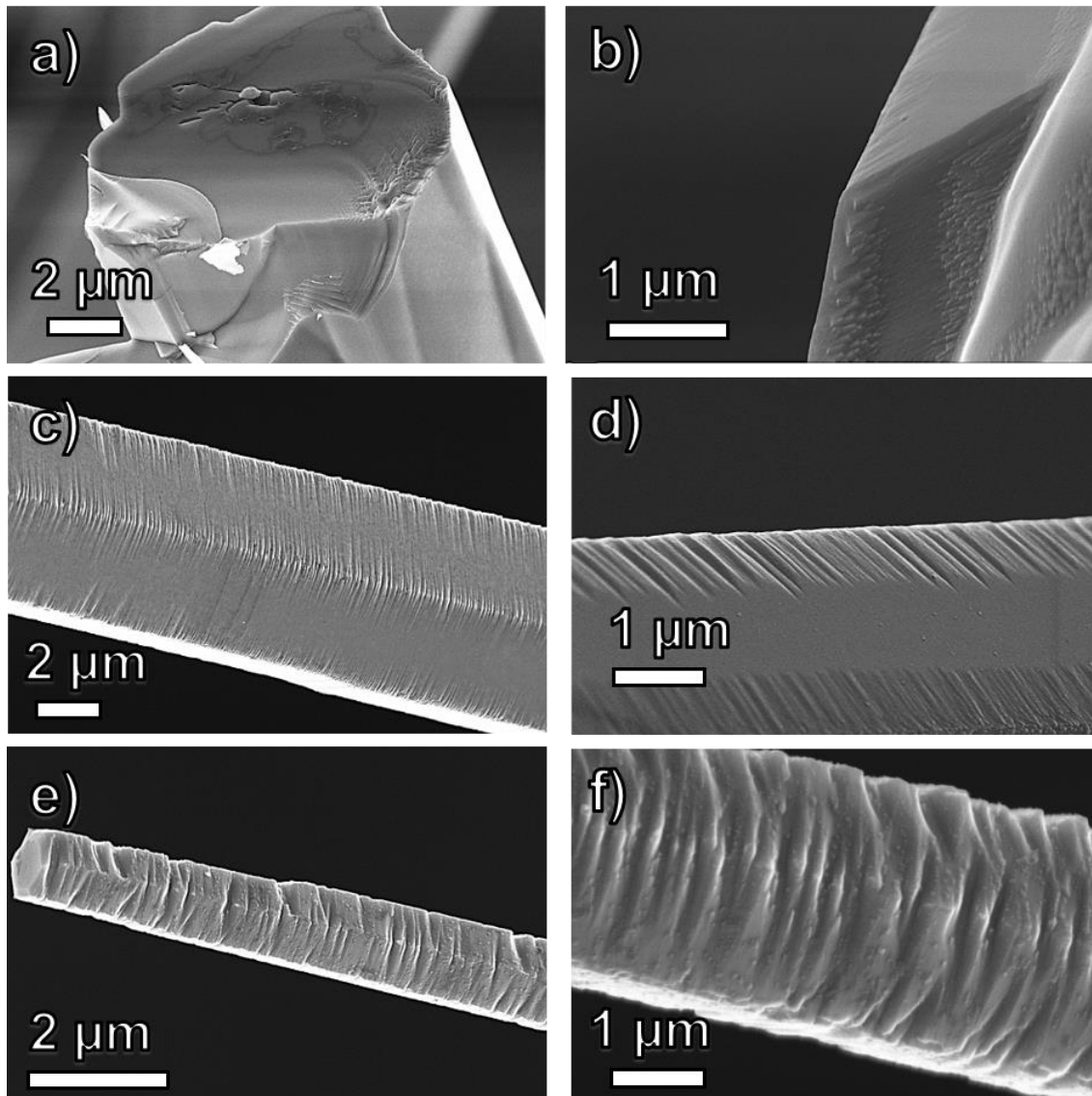


Figure 3. ZnO microwires after self-structuring during the photocatalysis: a) and b) – after 1 PC cycle, c) and d) after 2 PC cycles, e) and f) after 4 PC cycles. Closer look at the material's surface (b, d and f) reveals that the structured trenches develop a deeper profile, which increased with the number of PC cycles they were subjected to.

FIGURE 4

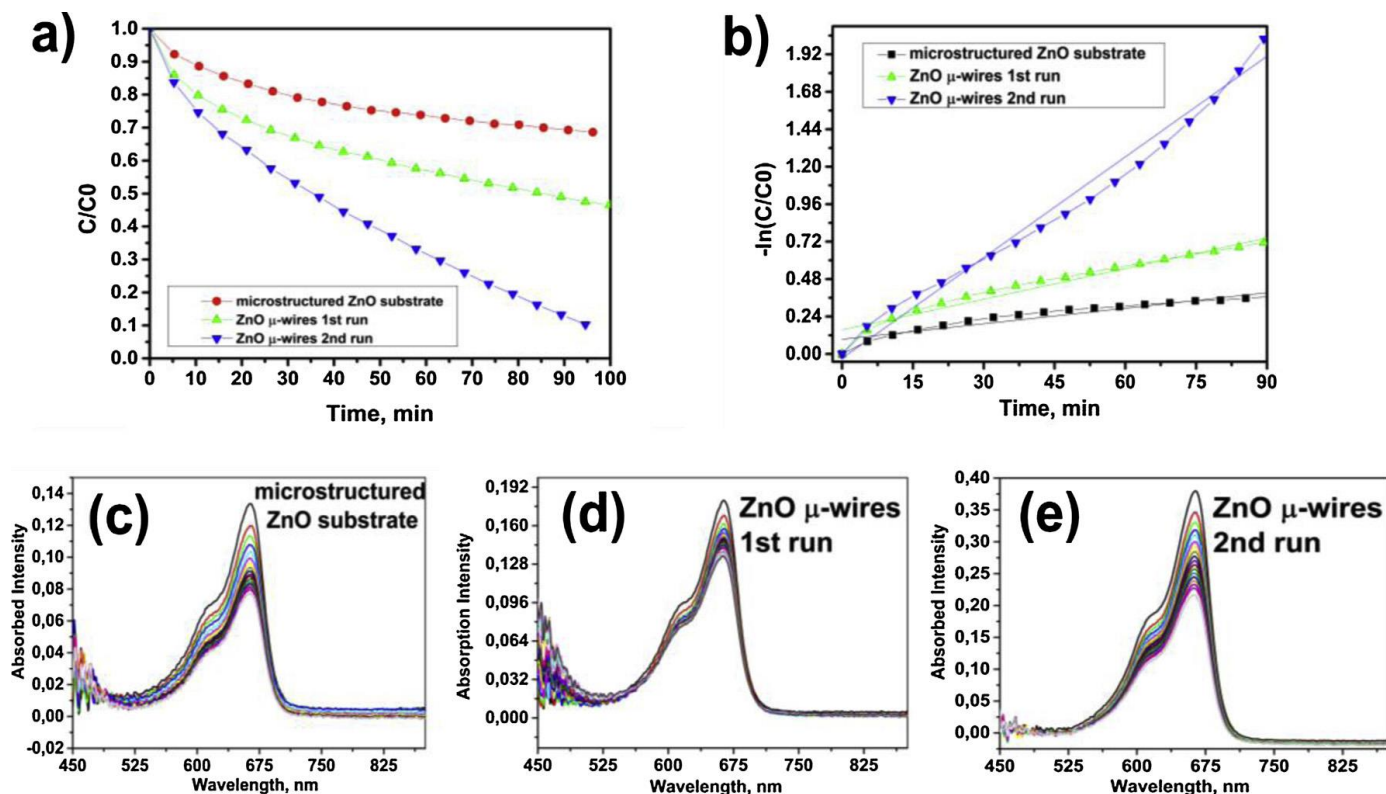


Figure 4. (a) Catalysis comparison of the degradation performance of ZnO microwires (μ -wires) with UV source turned on. Each spectrum was taken in 5 min intervals. PC performance of ZnO structures: microstructured ZnO substrate (red), as-grown ZnO μ -wires first cycle (green) and as-grown ZnO μ -wires (blue) in the second cycle. For all the curves a C/C_0 ratio in (a) and $-\ln(C/C_0)$ ratio in (b) was calculated, where C_0 is the initial concentration of MB (in absorption %) and C is a measured value of MB concentration in time intervals of 5 min. For each of the structure types mentioned in (a) and (b) the UV-Visible measured spectral data (with 5 min interval) is depicted in (c)-(e) accordingly.

FIGURE 5

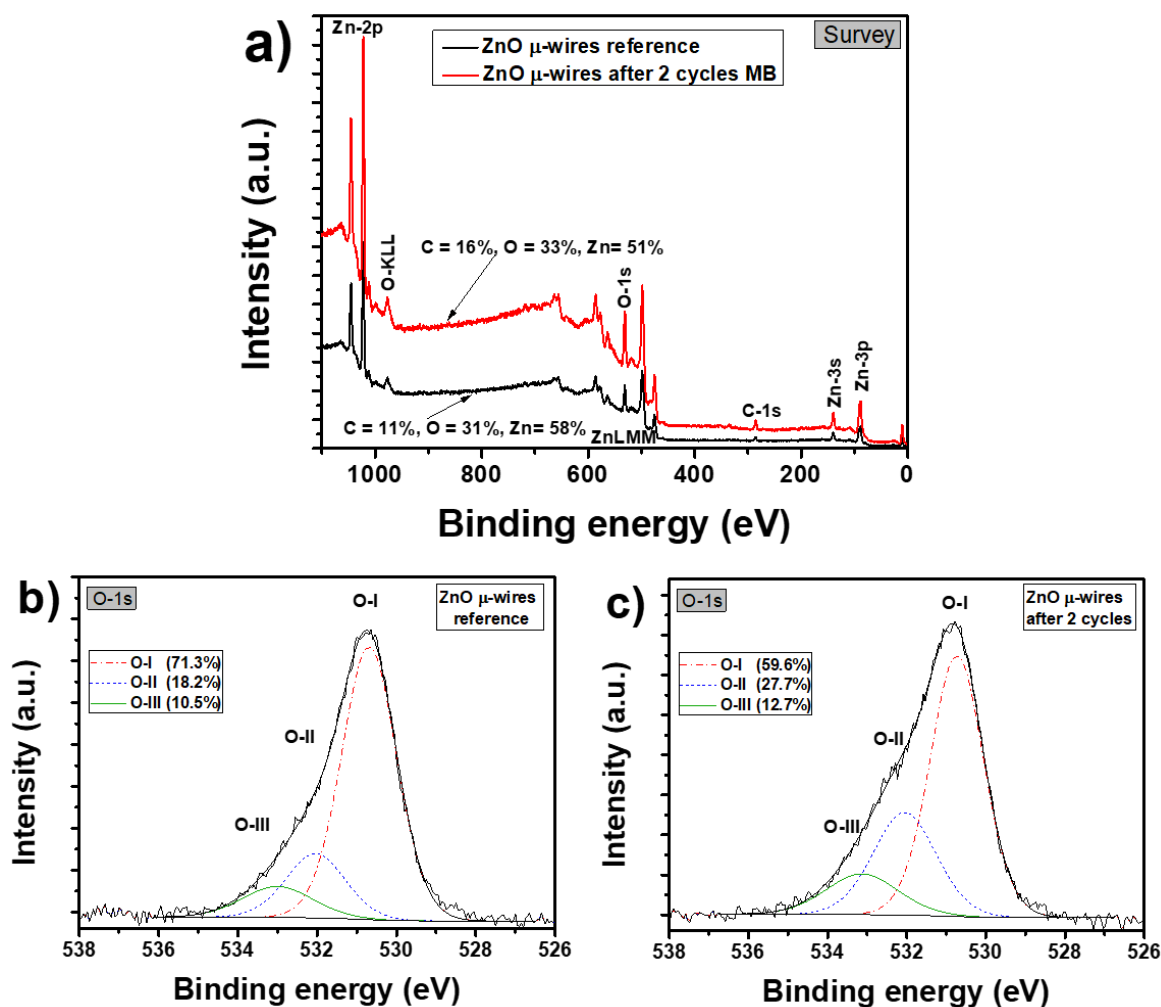


Figure 5. The results of XPS measurements: a) survey spectra together with at% concentrations of a ZnO μ -wires reference sample and ZnO μ -wires sample after two MB cycles; b) and c) high resolution O-1s spectra including peak deconvolution for the ZnO reference and cycled sample, respectively.

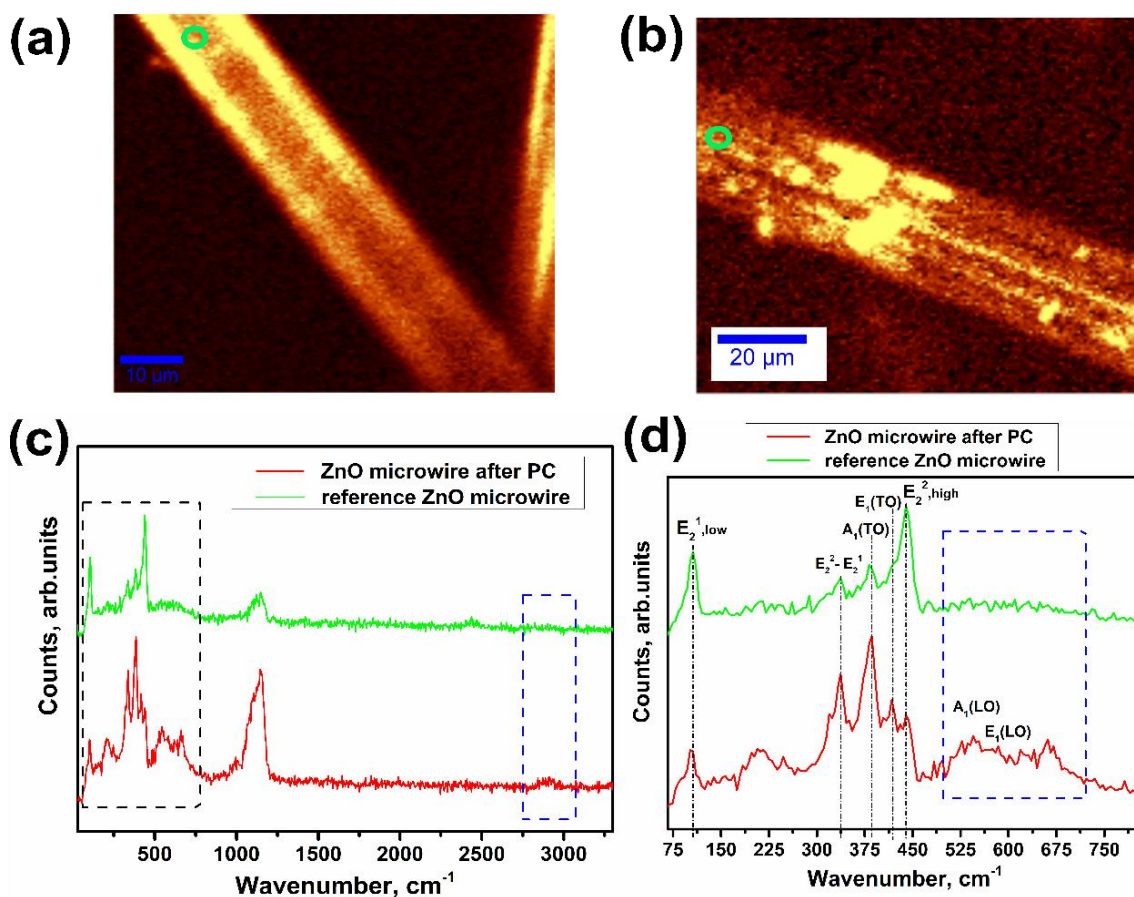
FIGURE 6

Figure 6. Raman spectroscopy of a reference ZnO microwire and a microwire after 2 cycles of MB photocatalysis. (a, b) Surface scans over ZnO needles. (c) Comparative Raman spectra taken from points marked with green circles in the surface scans (a) and (b). Blue marked region in (c) shows the organic residues present in the microwire after 2 MB decomposition cycles. Black dotted square indicates the region that a magnified image is taken from. (d) Magnified single spectra for k values $75\text{-}800\text{ cm}^{-1}$. Here the peaks $E_{2,low}^1$, $E_{2,high}^2$, $A_1(TO)$, $E_1(TO)$, $E_2^1-E_2^1$, $A_1(LO)$ and $E_1(LO)$ are marked with dashed lines. Blue dotted square indicates the region where the $A_1(LO)$ and $E_1(LO)$ become more pronounced for the treated ZnO microwires.

FIGURE 7

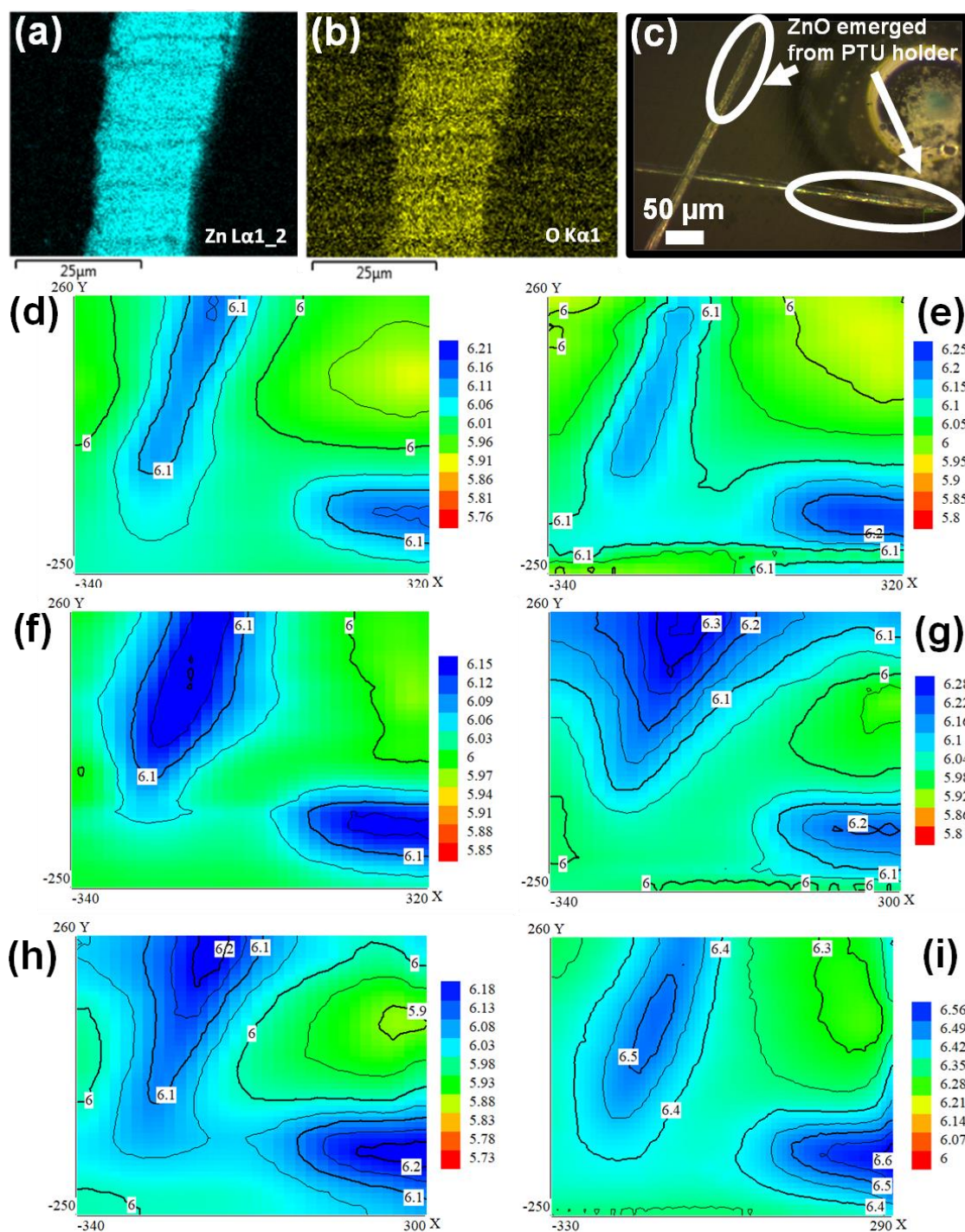


Figure 7. EDX maps (Zn and O) of polished ZnO - PTU samples with ZnO surface exposed for the reactions (a,b). (c) Light microscopy images of the pH mapping area. Selected pH maps on ZnO needles embedded into a PTU matrix with PC happening at ZnO surface exposed to MB solution and UV illumination (d-f) and relaxation process after UV is switched off (g-i). pH values corresponding to a color in the map is indicated on the right side of the corresponding map. Time sequences were taken after 25 min (d), 1 h (e) and 1.5 h (f) with UV illumination being switched on. Chosen relaxation sequences were taken after 1 h (g), 1.5 h (h) and 16.5 h (i) after UV source was turned off. The size of each pH map in microns is shown in X and Y axes. Please note that the pH maps have slightly different scale to better highlight the area of local pH changes.

Table I: Atomic concentration of chemical elements for reference and MB cycled sample (Carbon content excluded for the calculations)

| | Zn, at % | O, at% |
|---------------------------------|----------|--------|
| ZnO μ -wires (reference) | 65 | 35 |
| ZnO μ -wires after 2 cycles | 61 | 39 |

Table II: Relative concentrations of O-I, O-II and O-III components based on deconvolution of high-resolution O-1s peaks

| | ZnO μ -wires (reference) | ZnO μ -wires after 2 cycles |
|-------------|------------------------------|---------------------------------|
| O-I, at % | 71.3 | 59.6 |
| O-II, at% | 18.2 | 27.7 |
| O-III, at % | 10.5 | 12.7 |

Table III: Rate constants for different ZnO catalyst structures

| | ZnO | | |
|--|-------------------------------|-------------------------------|------------------------------|
| | microstructured substrate | microwires first run | microwires second run |
| Rate constant k_{abs} , [min ⁻¹] | 0.00332±2.61*10 ⁻⁴ | 0.00654±3.44*10 ⁻⁴ | 0.0215±8.23*10 ⁻⁴ |

Table IV: Parameters for the linear fitting of the $-\ln(C/C_0)$ coefficient

| Equation | $y = a + b*x$ | | |
|--|--|---|---|
| Weight | No Weighting | | |
| | <i>Flat ZnO substrate with 2D ZnO structures</i> | <i>ZnO microwires, 1st run</i> | <i>ZnO microwires, 2nd run</i> |
| Residual Sum of Squares | 0.01884 | 0.03924 | 0.18132 |
| Pearson's r | 0.95117 | 0.97588 | 0.98777 |
| Adj. R-Square | 0.89912 | 0.9497 | 0.97425 |
| $-\ln(C/C_0)$ | | Value | Standard Error |
| <i>Flat ZnO substrate with 2D ZnO structures</i> | Intercept | 0.09392 | 0.01469 |
| | Slope | 0.00332 | 2.60938E-4 |
| <i>ZnO microwires, 1st run</i> | Intercept | 0.15399 | 0.02012 |
| | Slope | 0.00654 | 3.44625E-4 |
| <i>ZnO microwires, 2nd run</i> | Intercept | -0.02739 | 0.04558 |
| | Slope | 0.0215 | 8.23335E-4 |